

Title:

Evolution of the lattice defects and crystalline domain size in carbon nanotube metal matrix composites processed by severe plastic deformation

Authors:

Katherine Aristizabal, Andreas Katzensteiner, Matteo Leoni, Frank Mücklich, Sebastian Suárez

This is the accepted manuscript of an article published in *Materials Characterization* (Volume 154, August 2019, Pages 344-352), DOI: 10.1016/j.matchar.2019.06.019

The version of record is available online at: <https://doi.org/10.1016/j.matchar.2019.06.019>

This manuscript is distributed under the terms and conditions of the Creative Commons License CC BY-NC-ND 4.0 (<https://creativecommons.org/licenses/by-nc-nd/4.0/>).



Evolution of the Lattice Defects and Crystalline Domain Size in Carbon nanotube Metal Matrix Composites processed by Severe Plastic Deformation

Abstract

Nickel (Ni) and carbon nanotube (CNT)-reinforced Ni-matrix composites were processed by high-pressure torsion (HPT). The evolution of dislocation densities and crystalline domain sizes were analyzed by means of X-ray diffraction (XRD) using Whole Powder Pattern Modelling (WPPM). The composites showed an evident gradient in the microstructural refinement and in hardness with increasing applied strain. This effect was found to be more pronounced in the presence of higher amounts of CNT. In particular, a higher amount of screw dislocations was measured by WPPM after HPT. It was concluded that the strengthening of CNT-MMC processed by HPT is mainly due to work hardening and grain refinement, both mechanisms being assisted by the presence of CNT, with marginal contribution of particle strengthening.

Keywords: Metal matrix composites (MMCs); Severe Plastic Deformation (SPD); X-ray diffraction (XRD); Lattice defects; Carbon nanotubes (CNT).

1. Introduction

It is well known that during severe plastic deformation (SPD) there is an increase in the dislocation density and high-angle grain boundaries, leading to the refinement of the microstructure [1]. Particularly in high pressure torsion (HPT), a microstructural gradient is observed in the sample (along the radial direction), which decreases gradually with increasing imposed strain until the saturation in the microstructural refinement is reached [2,3]. In the case of pure Ni, the equivalent von Mises strain ε_v needed to reach the onset of saturation in the microstructural refinement, characterized by a fairly constant hardness throughout the sample, is approximately $\varepsilon_v \sim 20$ [3]. In the disk center, on the other hand, stress homogeneity is not really obtained [4]. Nevertheless, although the equivalent strain there should be zero, according to $\varepsilon_v = \frac{2\pi Tr}{t\sqrt{3}}$, where T is the number of turns, t is the sample thickness and r the distance from the center of the sample [5], the dislocation density should increase due to the accumulated stress, especially in the case of pure metals, in which impurities are not expected to influence the microstructural evolution during processing. Furthermore, as dislocation glide is a very important deformation mechanism during HPT [4], a thorough analysis of the dislocation density in severely deformed CNT/Ni composites is of great interest, in order to better understand the remarkable increase in hardness [6] and the premature cracking during the deformation process at room temperature in the presence of high amounts of CNT [7]. Nevertheless, and to the best knowledge of the authors, there are still limited studies in the literature regarding the microstructural evolution of severely deformed metal matrix composites (MMC).

Structural and microstructural information, including crystalline domain sizes and dislocation densities, have been extracted from diffraction patterns by means of line profile analysis (LPA) using traditional approaches such as the Scherrer equation [8], the Warren-Averbach method [9] and Williamson-Hall plot [10]. Furthermore, semi-quantitative studies based on the modified approaches of these traditional techniques are common [11–16], which take into account the anisotropic nature of the dislocation strain field by considering the so-called dislocations contrast factor. Nevertheless, most of these techniques are limited to the extraction of microstructural information from the peak widths, by fitting each reflection with an arbitrary bell-shaped function; all other diffraction pattern details, albeit potentially important, are disregarded. To remove this limitation, full pattern analysis techniques such as the Whole Powder Pattern Modelling (WPPM), have been proposed [17]. In WPPM, the line profiles are obtained from physical models of the instrument and from the specimen. Specifically, the peak shape originating from dislocation effects is obtained according to the Wilkens-Krivoglaz-Ryaboshapka theory [18] that originally introduced the contrast factor of dislocations. Furthermore, dislocation densities analyzed by LPA techniques have been reported in the literature for severely deformed metals, whose high dislocation densities ($\rho > 10^{14} \text{ m}^{-2}$) cannot be easily quantified by means of traditional techniques such as Transmission Electron Microscopy (TEM); in many cases, conventional LPA is performed to obtain crystalline domain size and micro-strain, from which the dislocation density is calculated via the Williamson-Smallman approach [19–21], which is only valid for random distribution of dislocations (i.e. non-interacting dislocations).

The present study provides a systematic approach, in which WPPM is performed at two different positions on HPT deformed CNT/Ni composites as well on bulk Ni samples, by limiting the measured area along the radial direction and thus reducing the effect of the microstructural gradients on the results, in order to investigate the effect of increasing CNT content and increasing strain on the evolution of the domain size and dislocation densities during HPT. Finally, the strengthening contributions from grain boundaries, dislocation accumulation and the presence of particles were estimated from the results.

2. Materials and methods

The starting materials included multi-walled CNT (CCVD grown, Graphene Supermarket, USA density 1.84 g/cm^3) and dendritic Ni powder (Alfa Aesar, Germany mesh -325, 99.8% purity). Powder mixtures obtained via colloidal mixing (see e.g. [22]) were cold pressed (990 MPa) into cylindrical pellets (diameter 8 mm, thickness $\sim 1 \text{ mm}$) and sintered under vacuum ($2.0 \times 10^{-6} \text{ mbar}$) at $900 \text{ }^\circ\text{C}$ for 3 h. Different CNT fractions were used, namely: 0.5, 1, and 2 wt. % (2.4, 4.7 and 9 vol. %, respectively). All sintered samples ($\sim 1 \text{ mm}$ thickness and 8 mm of diameter) were further processed by means of HPT at room temperature using 1, 4, 10 and 20 T (turns), 4 GPa of pressure and 2 rpm. Pure Ni bulk samples were also obtained and processed under the same conditions and analyzed for comparison reasons, given that Ni has been extensively investigated and serves as model material for the HPT processing of MMC.

TEM micrographs were collected on selected samples using a JEOL JEM 2010 instrument operated at 200 kV. Specifically, Ni and 2 wt. % CNT samples processed using

1 T and 20 T were analyzed at 3 mm from the center. The TEM lamellas were extracted perpendicular to the shear direction in a dual-beam Helios NanoLab 600 (FEI) microscope using a gallium focused ion beam (FIB).

The HPT samples were cut in halves, embedded in resin, polished using polishing discs with 6, 3 and 1 μm diamond suspensions and mirror-finished with OP-S (Struers) colloidal silica. In this way, possible effects of the sample roughness on the results are avoided. The X-ray diffractograms were collected using $\text{Cu-K}\alpha$ radiation at room temperature by means of a PANalytical Empyrean diffractometer, equipped with a 50 μm focusing polycapillary collimator in the primary beam, and a parallel plate collimator (0.27° acceptance angle) in the diffracted beam. A Ni filter was used to suppress the unwanted $\text{K}\beta$ radiation. In this setup, only the lattice planes parallel to the surface of the specimen, i.e. orthogonal to the scattering vector \vec{s} , contribute to the diffracted signal. In order to limit the effects of the microstructural gradients on the results, the beam size was restricted to a width of 50 μm and a variable length depending of the 2θ angle, e.g. 146.19 μm at 40° and 65.27 μm at 100°. In order to better correlate the results to the specific equivalent strains corresponding to the measured areas located at about 3 mm from the center, the specimen was aligned such that the scattering vector was parallel to the shear direction and in this way, although the X-ray penetration depth in Ni varies from 34.28 μm at 40° and 52.52 μm at 100°, the microstructural gradient along the depth is expected to be negligible.

Only the peaks corresponding to *fcc* Ni were observed in the 40°-100° scan range. The step size was set to 0.05° with 40 seconds counting time for a total of 1200 points.

Figure 1 shows a schematic representation of the XRD setup. The LaB₆ instrumental profile powder standard was also measured with the same configuration in order to model the instrumental broadening, using an oscillation of the stage of 5 mm in the X axis to increase the counting statistics and reduce the graininess problems (the LaB₆ powder has in fact a particle size of ca. 2 μm and the particles are almost single crystals).

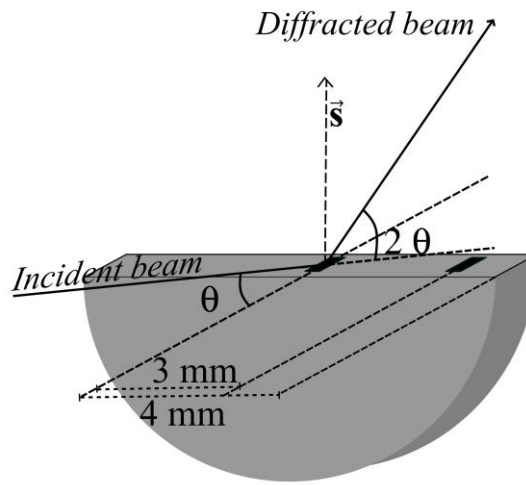


Figure 1 X-Ray Diffraction in Bragg Brentano configuration used in the present study.

For the analysis of the dislocation density and the crystalline domain size, the PM2K software, implementing the WPPM method, was employed [23,24]. A thorough description of the WPPM approach is given elsewhere [17]. In the following a short and simplified introduction to the method is given.

In WPPM, the complex function $C_{hkl}(L)$ describes the Fourier Transform (FT) of the intensity $I_{hkl}(d^*)$ of the hkl diffraction profile. If d^* is a length in reciprocal space (equal to d_{hkl}^* in the Bragg condition), then

$$I_{hkl}(d^*) = k_{hkl}(d^*) \int C_{hkl}(L) \exp(2\pi L(d^* - d_{hkl}^*)) dL \quad (1)$$

Here, $k_{hkl}(d^*)$ comprises all terms contributing to $I_{hkl}(d^*)$ and not related to line broadening sources, such as Lorenz-polarization factor, the structure factor, scale factor, etc. As broadening effects are convoluted in the measured diffraction profile and due to the properties of the Fourier transform of a convolution, $C_{hkl}(L)$ is a product of functions describing the various sources of broadening affecting the analyzed profile. In our case we have to consider, for instance, the instrumental broadening (T_{pV}^{IP}) that can be measured using a line-profile standard, the contribution from the finite size of the domains (A^S), the contribution from the lattice distortions caused by dislocations (A^D). Therefore,

$$C_{hkl}(L) = (T_{pV}^{IP}) \cdot (A^S) \cdot (A^D) \quad (2)$$

Expressions for the above mentioned FTs can be found in [17]. Further broadening sources can be included, when necessary.

The parameters of interest obtained in the WPPM analysis were: mean (μ) and square of the variance (σ) of a log-normal distribution of coherent domain sizes, dislocation density (ρ), and average character of the dislocations (extracted as f_e , relative edge fraction). Spherical domains were used to model the diffraction patterns of the HPT samples with a log-normal distribution of domains, which has been considered appropriate in the case of severely deformed metals [1].

For a quantitative evaluation of the dislocation densities, the (orientation-averaged) dislocation contrast factor is however needed for each individual hkl . The approach

proposed by Martinez-Garcia et al. [25] can be used in the general case. For cubic materials, the following holds [26]: $\bar{C}_{hkl} = A+BH$, with $H = \frac{(h^2k^2+h^2l^2+l^2h^2)}{(h^2+k^2+l^2)^2}$, and A and B are constants that depend on the dislocation slip system and on the single-crystal elastic constants of the material. The primary slip system of Ni is $\frac{1}{2}\langle 110 \rangle \{1\bar{1}1\}$. Suitable A and B values for edge and screw dislocations acting on this slip system were calculated from the known values proposed by Ungár et al. [11] obtained using the single elastic constants $c_{11} = 243.6$; $c_{12} = 149.4$ and $c_{44} = 119.6$ GPa (note that a different parameterization is used in the cited reference, and in particular that $A = \bar{C}_{h00}$, $B = -\frac{c_{44}}{A}$). The calculated values for edge dislocations are: $A_e = 0.262$, $B_e = -0.367$, and for screw dislocations: $A_s = 0.267$ and $B_s = -0.599$ in agreement with the data calculated by Scardi et al. [26].

Moreover, despite the technical difficulties related to the need of working with a small spot size and consequently, with a broad instrumental function, the agreement between data and model is rather good. As an example, Figure 2 shows the modelling result for Ni and 2 wt. % CNT samples processed to equivalent strains of $\varepsilon_v \sim 16$ and $\varepsilon_v \sim 320$, as representative examples. Moreover, the difference plot is almost featureless in all studied cases. Figure 2 shows that the addition of CNT to Ni causes evident line broadening with increasing strain.

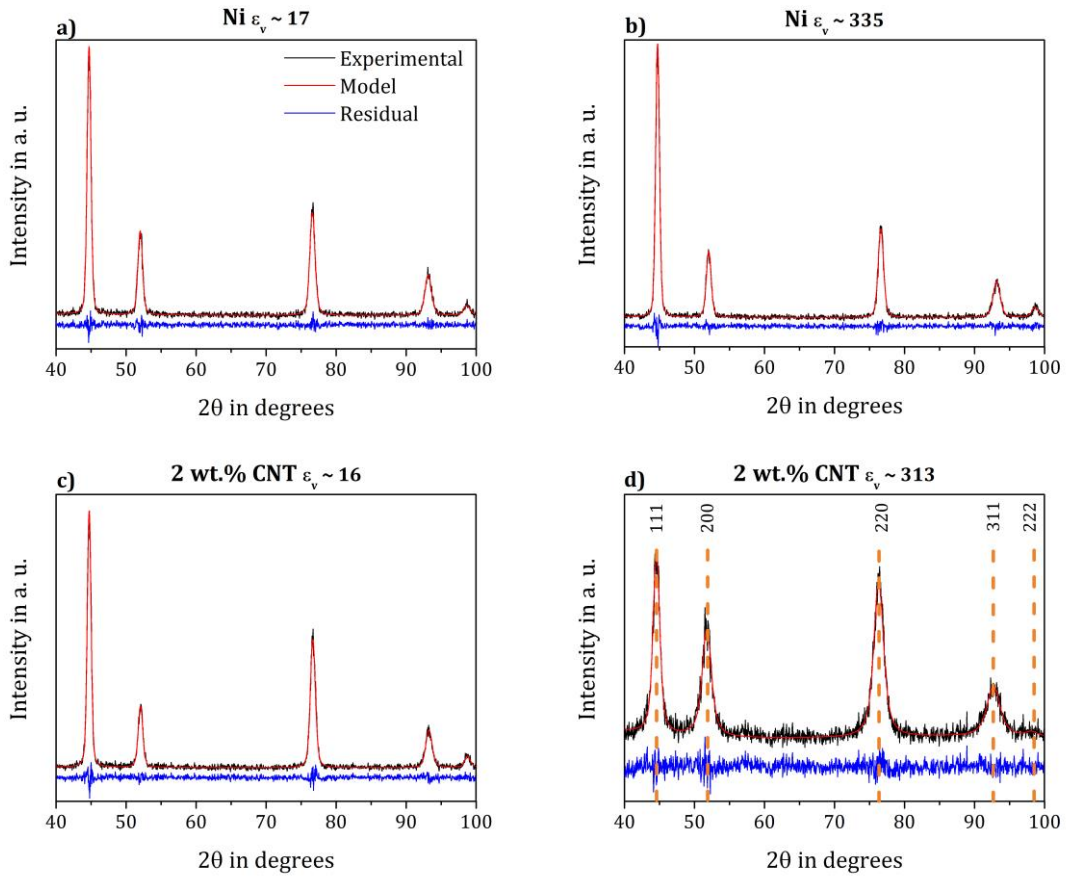


Figure 2 Examples of WPPM of the data collected at 3 mm from the center on a) Ni after 1 T and b) after 20 T, c) 2 wt. % CNT after 1 T and d) after 20 T.

In addition, Vickers micro hardness ($HV_{0.3}$) measurements were performed at 3 mm from the samples' centers using an indenter Struers DuraScan 50/70/80 using 15 s of dwell time.

3. Results and discussion

TEM micrographs in Figure 3 show exemplarily the effect of CNTs on the microstructural refinement with increasing applied strains. In contrast to pure Ni, where no

further grain refinement is observed from Figure 3e, the HPT applied to 2 wt. % CNT samples (Figure 3f) causes a significant decrease in grain size. Furthermore, oxide particles could also promote grain refinement by pinning the dislocation and grain boundary motion [27]. Nevertheless, a negligible contribution should be expected in this case in comparison to the effect provided by the CNTs. Note that the oxide signal is not detected as shown in the respective SAED patterns in Figure 3. Additionally, the introduction of oxygen during SPD is more likely to occur in powder samples [28] than in annealed (bulk) ones (this study).

The evolution of the mean domain size, as well as the dislocation density with increasing equivalent strains are presented in Figs. 4 and 5, respectively. The mean domain sizes D and the respective standard deviations SD (presented as the error bars), have been calculated from the mean (μ) and the square of the variance (σ) of the log-normal distributions via $D = e^{(\mu + \frac{\sigma^2}{2})}$ and $SD = \sqrt{(e^{(2\mu + \sigma^2)})(e^{\sigma^2} - 1)}$, respectively. In the case of the dislocation densities, the error bars correspond to the estimated errors in the WPPM.

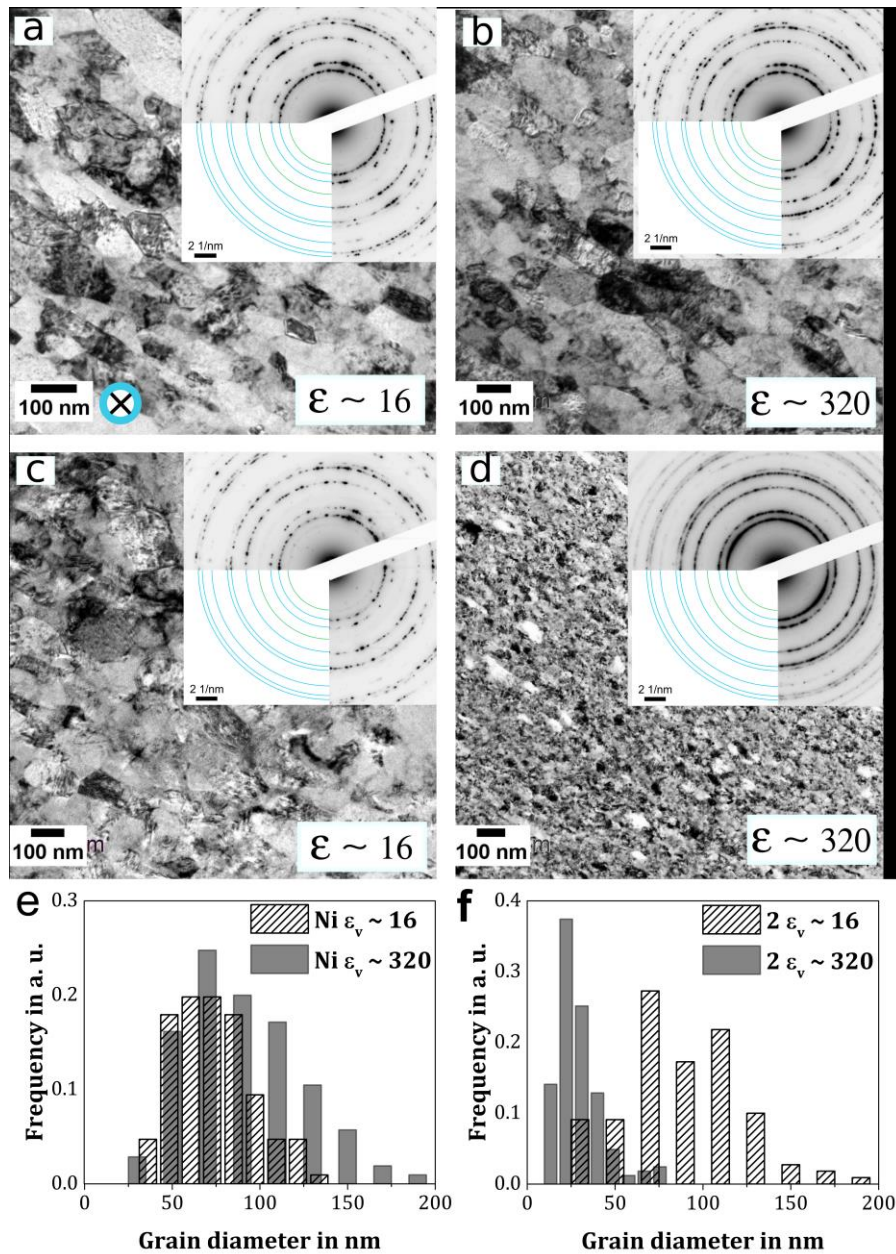


Figure 3 Bright Field TEM micrographs and respective SAED patterns of (a, b): Ni and (c, d): 2 wt. % CNT samples, processed to the respective equivalent strains, given on the micrographs. Shear direction normal to plane of paper (marked as X). (e, f): Grain size distributions of Ni and 2 wt. % CNT samples, respectively.

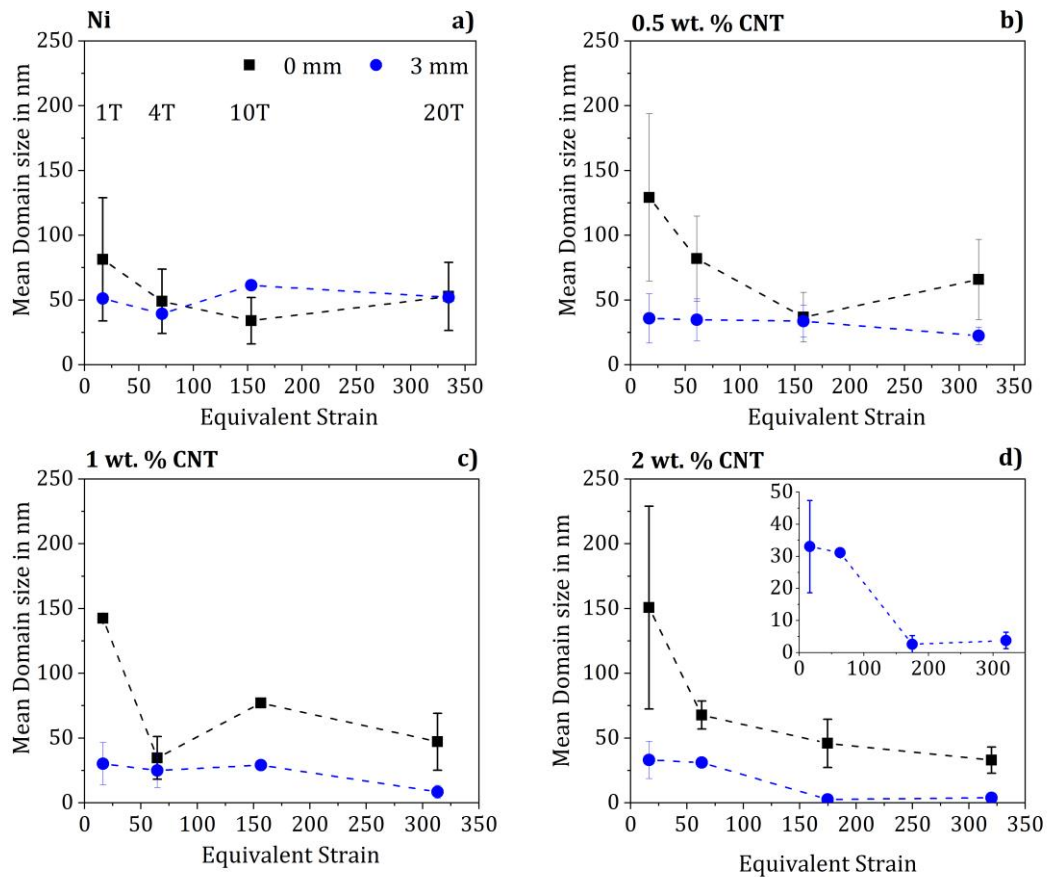


Figure 4 Evolution of mean domain size for increasing equivalent strains and increasing number of turns (for the case of samples' centers where the equivalent strain is zero) in a) Ni, b) 0.5 wt. % CNT, c) 1 wt. % CNT and d) 2 wt. % CNT.

Regarding the composites, the distribution of the reinforcement at the disks' centers is expected to be less homogeneous than at areas further away from it since the reinforcement distribution should improve with increasing equivalent strain and increasing CNT content [29]. Moreover, since the grain size is expected to reduce with increasing accumulated strain, a reduction in the domain sizes is expected further away from the

samples' centers, especially in the composites, where the presence of second phases can enhance the refinement process. This effect can be observed in Figure 4.

On one hand, the reduction in the domain size caused by the presence of CNT in the composites can be explained analogically to the reduction in grain size caused by impurities. It is well known that edge dislocations interact more effectively with solute atoms than screw dislocations. For instance, when edge dislocations interact with solute atoms inside the grains (such as dissolved oxygen atoms), they are pinned by them [28]. These pinning effect can eventually promote dislocation pile-up and subsequently dislocation rearrangement into low energy configurations (LAGB), which not only increases the dislocation density but also assists the microstructural refinement. At the same time, dislocations may interact with solute atoms and second phases at the grain boundaries. Additionally, as the steady state is ruled by the grain boundary mobility [3], the decrease in steady state grain size can be accounted by the pinning of the grain boundaries by impurities and second phase particles located there.

On the other hand, in the case of pure bulk Ni samples, processing above the equivalent strain needed for the saturation hardness to take place (i.e. $\varepsilon_v \sim 20$, see Figure 6), leads to marginal changes in both the domain size and the dislocation density. No further decrease in the domain size might be related to a transient state, which involves dislocation pileup at the grain boundaries and grain boundary motion as discussed by Pippan et al [3], who studied the evolution of the grain size of Ni samples subjected to HPT at room temperature starting from both coarse and nano grained samples, obtaining the same final steady state grain size after HPT. According to them, during SPD, pure metals are not

further refined after the steady state has been reached due to stress-induced boundary migration phenomena. Furthermore, they estimated a saturation size of plastically deformed Ni of about 200 nm (as measured from TEM micrographs) [3]. In the present study, Ni average grain sizes extracted from TEM micrographs are in the order of ~ 80 nm (see Figure 3e), which are in the same order to the sizes extracted from WPPM for the respective samples (see Figure 4a). However, the domains "seen" by diffraction should not be confused with the grains observed by microscopy: the two are the same only when the "grains" are defect-free, contain a non-significant quantity of defects, or defects are randomly distributed within the grains.

The dislocation density of the bulk Ni samples from the present study is consistent with the results reported in [30] for HPT Ni, namely $\rho \sim 0.3 \times 10^{16} \text{ m}^{-2}$ (Figure 5a). On the other hand, the dislocation density increases in the composites with increasing applied strains and increasing CNT content. Specifically, adding CNTs to a Ni matrix leads to a significant increase in the dislocation density up to $\rho \sim 4 \times 10^{16} \text{ m}^{-2}$ at 3 mm from the center (Figure 5), which can be in turn observed as an increase in hardness (see Figure 6). Additionally, the difference in dislocation density between the center and the edge also increases with increasing strain and CNT content, which is related to an effective pinning of the grain boundaries by the CNT and possible delay in dislocation accumulation at the samples' centers during HPT.

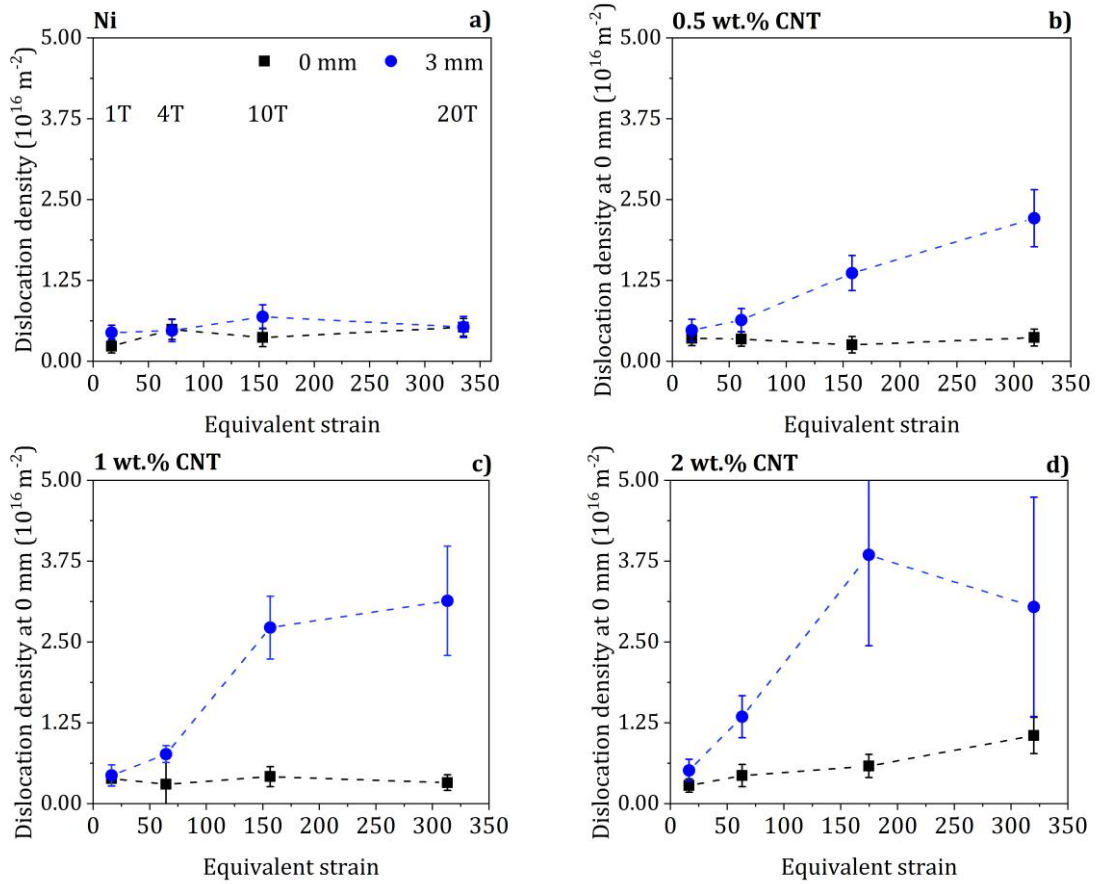


Figure 5 Evolution of the dislocation density for increasing equivalent strains and increasing number of turns (for the case of samples' centers where the equivalent strain is zero) in a) Ni, b) 0.5 wt. % CNT, c) 1 wt. % CNT and d) 2 wt. % CNT.

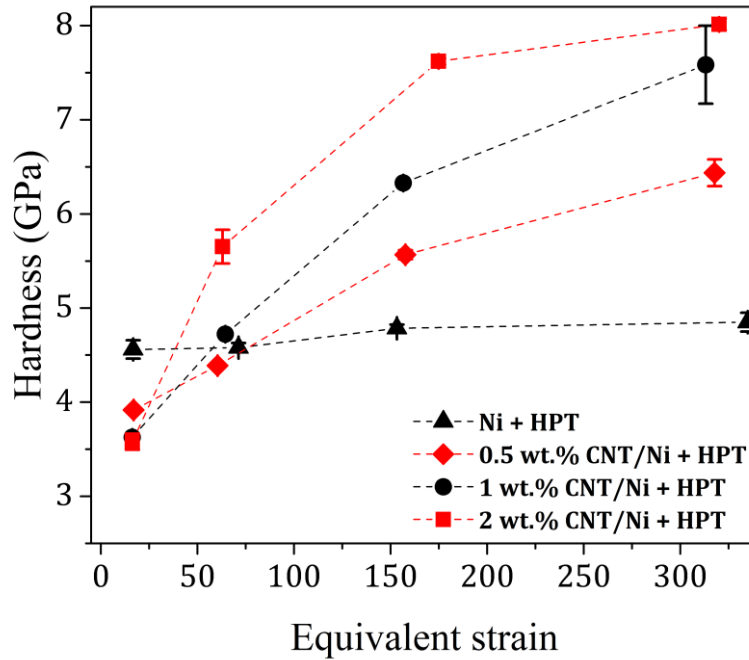


Figure 6 Evolution of hardness (measured at 3 mm from the samples' centers) with increasing equivalent strains.

Furthermore, the evolution of the dislocation character, as described by the edge dislocation fraction f_e obtained from WPPM, is reported in Figure 7 for the two studied sample's positions. It is observed that mainly screw dislocations accumulate far from the center during processing in both Ni samples and the composites. This can be explained as during plastic deformation, mainly dislocation tangles of edge character are arranging to form dislocation walls and screw dislocations locate primarily in the grain interiors and can be easily annihilated by cross slip [31–33]. Moreover, the application of high hydrostatic pressures during HPT mostly restricts the deformation-induced vacancies to reach the edge dislocations, reducing effectively dislocation climb and annihilation [34,35]. By enhancing the dislocation density, there is an increase in the total grain boundary area, which

corresponds to a decrease in the average grain size [36] that is equivalent to a decrease in the crystallite size as measured by XPA. Moreover, J. Gubicza et al [37], suggested that the annihilation of both edge and screw dislocations is hindered during HPT more effectively in comparison to other SPD processing methods due to the high load applied, which delays both climb and cross-slip of dislocations. According to this, the increase in the screw dislocation character can be explained by the cross-slip of dislocations being hindered during HPT, with edge dislocations mainly arranging to contribute to the grain refinement of the material. Moreover, after releasing the hydrostatic pressure applied during processing, a release of excess vacancy concentration takes place as proposed in [38], which promotes some dislocation annihilation, especially of edge character. In the sample's center the strain accumulates due to the inhomogeneous nature of the HPT process. Therefore, given that low misorientation angles of subgrains and even dipolar dislocation walls separating subgrains with no differences in orientation are "viewed" by XRD as crystalline domains [39], when the available edge dislocations arrange with increasing imposed strain into dislocation cells and sub-grains, these are in turn "seen" by XRD as new crystalline domains, which reduces the detection of edge dislocations located there.

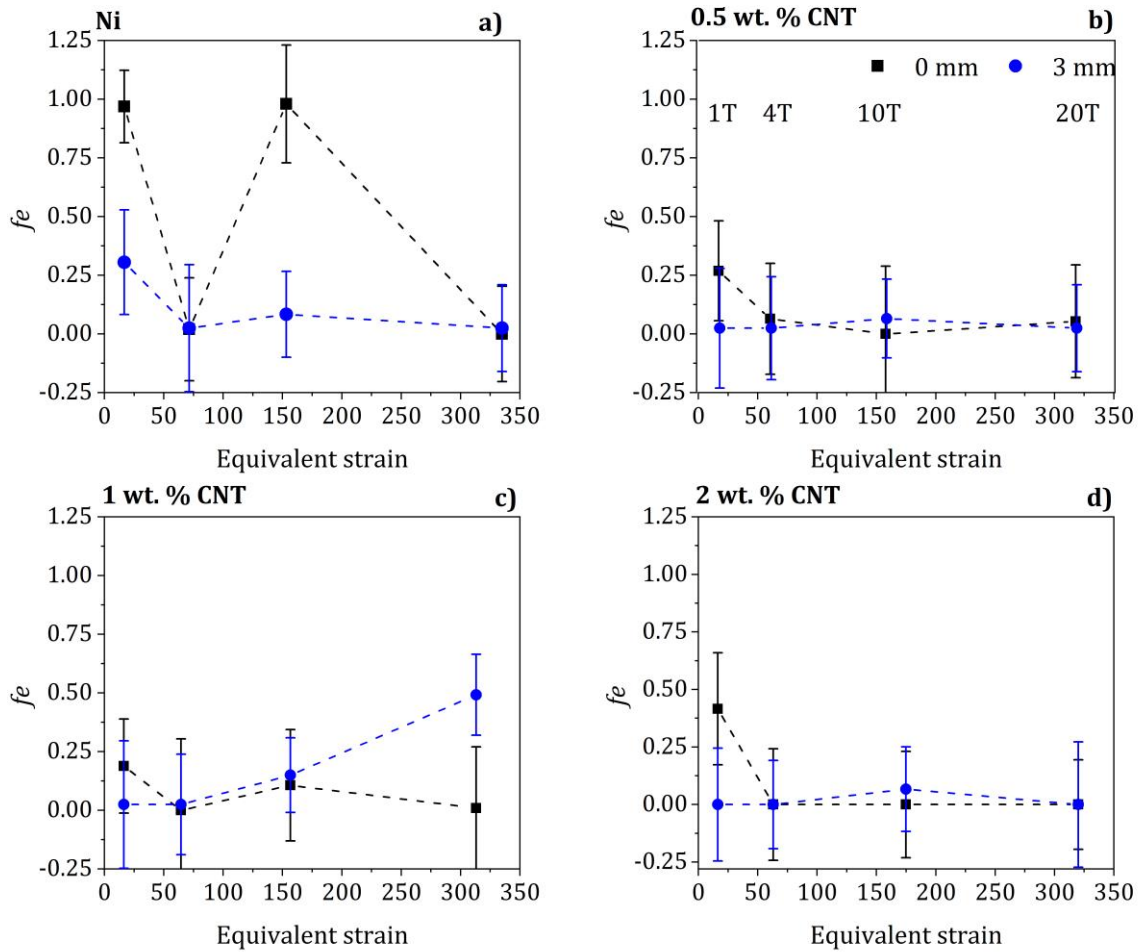


Figure 7 Evolution of the edge dislocation fraction for increasing equivalent strains and increasing number of turns (for the case of samples' centers where the equivalent strain is zero) in a) Ni, b) 0.5 wt. % CNT, c) 1 wt. % CNT and d) 2 wt. % CNT.

Finally, different strengthening mechanisms can be accounted for the increase in hardness in the severely deformed composites such as strain hardening, grain size refinement (Hall-Petch) and dispersion strengthening (Orowan). However, it was observed that even though increasing carbon content increases the saturation value of hardness in Ni samples during HPT [40], increasing CNT content up to 2 wt.% yielded similar saturation

values of hardness in samples processed at room temperature, as opposed to higher processing temperatures, where CNT play an important role [7]. Moreover, it was observed that the increase in hardness of CNT-reinforced MMC followed a Hall-Petch relationship with small deviations at smaller grain sizes [7]. Nevertheless, as stated in [41], unless significant recovery of defects post deformation (or during deformation) occurs, there will be a correlation between dislocation density and the grain size and thus the linearity of a Hall-Petch type plot should not be taken as an indication that grain boundary strengthening dominates. The contribution of these three mechanisms to the strengthening was estimated and plotted in Figure 8. Other contributions are considered negligible in comparison.

For the estimation of the grain boundary contribution via the Hall-Petch relation, it was assumed that crystalline domains act as obstacles for dislocation analogous to grain boundaries according to $\Delta\sigma = K \frac{1}{\sqrt{D}}$, where K was taken from the data compiled in [42] for nano-crystalline Ni assuming $\Delta\sigma = \frac{1}{3}\Delta\text{Hardness}$. Furthermore, the contribution of dislocation strengthening (work hardening) was estimated using the Taylor relation $\Delta\sigma = M\alpha Gb\sqrt{\rho}$, where M is the Taylor factor (~ 3), α is a constant taken as 0.24, G is the shear modulus $G=76.5$ GPa, b is the Burgers vector $b=0.249$ nm and ρ is the total dislocation density. Dispersion hardening due to the presence of CNT was estimated using the Orowan-Ashby relation $\Delta\sigma = \frac{0.13Gb}{d} \ln \frac{r}{b}$ [43], where d is the inter-particle distance, which was taken as the nearest neighbor distance calculated from the distance of the agglomerates centers of mass as described in [29], and r was taken as the agglomerate radius. It should be noted that

the strengthening contributions remain an estimation and should not be taken as absolute values.

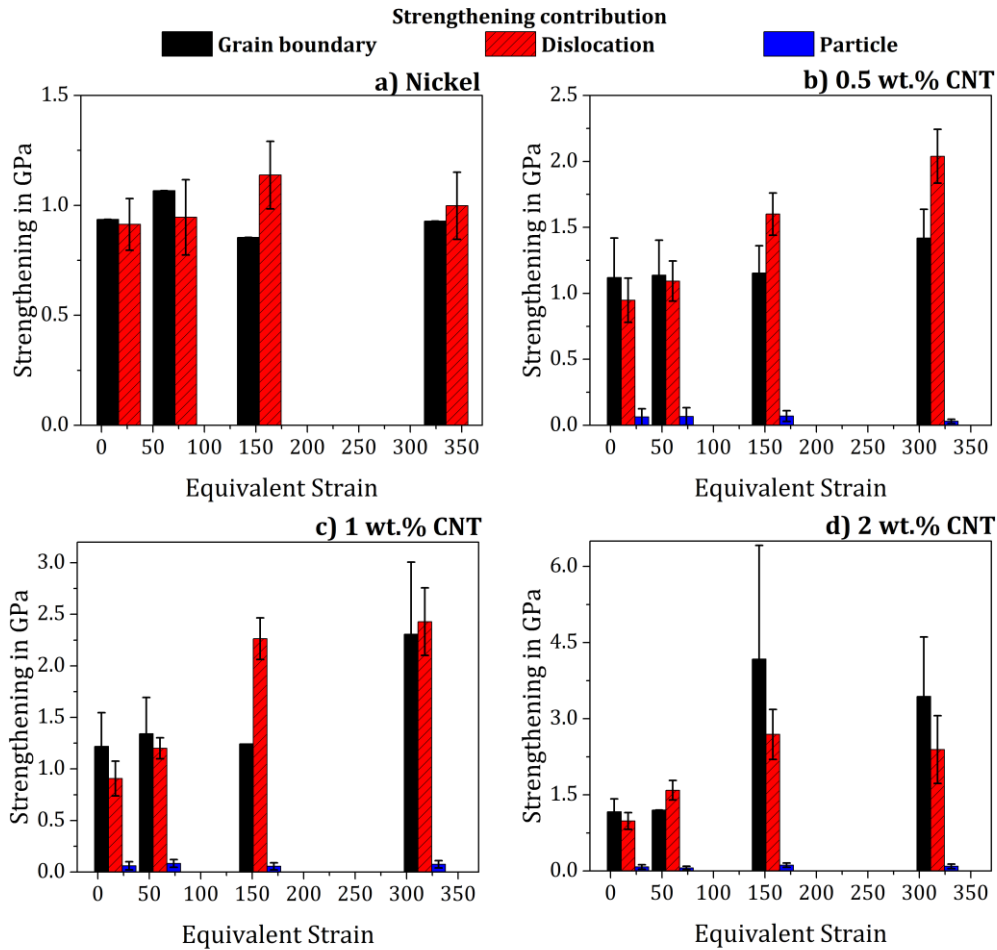


Figure 8 Contribution from the respective strengthening mechanisms with increasing equivalent strains in in a) Ni, b) 0.5 wt. % CNT, c) 1 wt. % CNT and d) 2 wt. % CNT.

It has been shown that both work hardening and grain boundaries contribute to the strengthening in many metals [44] and composites [45] processed by SPD. This correlates well with the present results. Nevertheless, both dislocations and grain boundaries have comparable contribution to the strengthening, except where the domain sizes are the

smallest and grain boundaries dominate due to the significantly smaller fraction of dislocations that can be stored inside the grains. Orowan strengthening, on the other hand, has only small contribution to the strengthening mainly because, even though the CNT agglomerate sizes and homogeneity was significantly improved during HPT [29], the agglomerate size is still large (~100nm), which in many cases is bigger than the grain sizes, and because dislocation loops that may form around smaller agglomerates can eventually create dislocation cell structures, which in turn may result in a Hall-Petch type strengthening [43].

Based on the present results it can be concluded that the presence of CNT in CNT-MMC processed at room temperature by SPD with increasing CNT content and increasing imposed strain, increases the dislocation density (work hardening), assists the grain refinement and to a lesser extent contribute to particle strengthening via Orowan looping.

4. Conclusions

In summary, SPD of CNT/Ni matrix composites was studied by TEM and advanced X-ray diffraction analysis. The WPPM of diffraction data is capable of evidencing the variations in the microstructure of the specimens subjected to SPD and pointing out the microstructure refinement effect caused by the presence of CNT in the system. The saturation in the microstructural refinement is not reached during HPT at room temperature in the studied composites, as evidenced by the significant gradient in microstructure and hardness. Furthermore, an increase in the dislocation density in the system is evidenced with increasing number of turns. Moreover, the increase in the quantity of screw

dislocations measured by WPPM, was attributed to the reduction of restoration processes due to the high applied hydrostatic load during HPT of CNT/MMC, with mainly edge dislocations contributing to the grain refinement. Finally, CNT are observed to promote the grain refinement significantly, as a consequence of the interaction of the nanotubes with grain boundaries and dislocations, which contribute significantly to the strengthening of the composites.

Acknowledgements

K. Aristizabal wishes to thank the German Academic Exchange Service (DAAD) (91567148) for their financial support. S. Suarez and K. Aristizabal gratefully acknowledge the financial support from DFG (Grant: SU911/1-1). A. Katzensteiner gratefully acknowledges the financial support by the Austrian Science Fund (FWF): I2294-N36. The authors want to gratefully acknowledge Sebastian Slawik for his continuing support and José Javier Rico for his assistance during the preparation of the initial materials. The X-ray diffractometer was financed by the DFG and the federal state government of Saarland INST 256/431-1 FUGG.

Conflict of interest

The authors declare no conflict of interest.

Data availability

Data will be provided upon reasonable request to the corresponding author.

References

- [1] R.Z. Valiev, R.K. Islamgaliev, I. V. Alexandrov, Bulk nanostructured materials from severe plastic deformation, *Prog. Mater. Sci.* 45 (2000) 103–189. doi:10.1016/S0079-6425(99)00007-9.
- [2] Y. Estrin, A. Molotnikov, C.H.J. Davies, R. Lapovok, Strain gradient plasticity modelling of high-pressure torsion, *J. Mech. Phys. Solids.* 56 (2008) 1186–1202. doi:10.1016/j.jmps.2007.10.004.
- [3] R. Pippan, S. Scheriau, A. Taylor, M. Hafok, A. Hohenwarter, A. Bachmaier, Saturation of Fragmentation During Severe Plastic Deformation, *Annu. Rev. Mater. Res.* 40 (2010) 319–343. doi:10.1146/annurev-matsci-070909-104445.
- [4] H.W. Zhang, X. Huang, N. Hansen, Evolution of microstructural parameters and flow stresses toward limits in nickel deformed to ultra-high strains, *Acta Mater.* 56 (2008) 5451–5465. doi:10.1016/j.actamat.2008.07.040.
- [5] H.P. Stüwe, Equivalent strains in severe plastic deformation, *Adv. Eng. Mater.* 5 (2003) 291–295. doi:10.1002/adem.200310085.
- [6] K. Aristizabal, S. Suárez, A. Katzensteiner, A. Bachmaier, F. Mücklich, Evolution of the microstructure in carbon nanotube reinforced Nickel matrix composites processed by high-pressure torsion, *IOP Conf. Ser. Mater. Sci. Eng.* 258 (2017). doi:10.1088/1757-899X/258/1/012008.
- [7] A. Katzensteiner, T. Müller, K. Kormout, K. Aristizabal, S. Suarez, R. Pippan, A. Bachmaier, Influence of Processing Parameters on the Mechanical Properties of HPT-Deformed Nickel/Carbon Nanotube Composites, *Adv. Eng. Mater.* 1800422 (2018) 1800422. doi:10.1002/adem.201800422.
- [8] P. Scherrer, Bestimmung der Größe und der inneren Struktur von Kolloidteilchen mittels Röntgenstrahlen, *Nachrichten von Der Gesellschaft Der Wissenschaften Zu Göttingen, Math. Klasse.* (1918) 98–100. <http://resolver.sub.uni-goettingen.de/purl?GDZPPN002505045>.
- [9] B.E. Warren, B.L. Averbach, The effect of cold-work distortion on x-ray patterns, *J. Appl. Phys.* 21 (1950) 595–599. doi:10.1063/1.1699713.
- [10] G.K. Williamson, W.H. Hall, X-ray line broadening from filed aluminium and wolfram, *Acta Metall.* 1 (1953) 22–31. doi:10.1016/0001-6160(53)90006-6.
- [11] T. Ungár, I. Dragomir, Á. Révész, A. Borbély, The contrast factors of dislocations in cubic crystals: The dislocation model of strain anisotropy in practice, *J. Appl. Crystallogr.* 32 (1999) 992–1002. doi:10.1107/S0021889899009334.
- [12] P. Jenei, E.Y. Yoon, J. Gubicza, H.S. Kim, J.L. Lábár, T. Ungár, Microstructure and hardness of copper-carbon nanotube composites consolidated by High Pressure Torsion, *Mater. Sci. Eng. A.* 528 (2011) 4690–4695. doi:10.1016/j.msea.2011.02.066.

- [13] T. Shintani, Y. Murata, Evaluation of the dislocation density and dislocation character in cold rolled Type 304 steel determined by profile analysis of X-ray diffraction, *Acta Mater.* 59 (2011) 4314–4322. doi:10.1016/j.actamat.2011.03.055.
- [14] J. Gubicza, N.H. Nam, L. Balogh, R.J. Hellmig, V. V. Stolyarov, Y. Estrin, T. Ungár, Microstructure of severely deformed metals determined by X-ray peak profile analysis, *J. Alloys Compd.* 378 (2004) 248–252. doi:10.1016/j.jallcom.2003.11.162.
- [15] J. Gubicza, L. Balogh, R.J. Hellmig, Y. Estrin, T. Ungár, Dislocation structure and crystallite size in severely deformed copper by X-ray peak profile analysis, *Mater. Sci. Eng. A.* 400–401 (2005) 334–338. doi:10.1016/j.msea.2005.03.042.
- [16] T. Ungár, J. Gubicza, P. Hanák, I. Alexandrov, Densities and character of dislocations and size-distribution of subgrains in deformed metals by X-ray diffraction profile analysis, *Mater. Sci. Eng. A.* 319–321 (2001) 274–278. doi:10.1016/S0921-5093(01)01025-5.
- [17] P. Scardi, M. Leoni, Whole powder pattern modelling, *Acta Crystallogr. Sect. A Found. Crystallogr.* 58 (2002) 190–200. doi:10.1107/S0108767301021298.
- [18] M. A. Krivoglaz, *X-Ray and Neutron Diffraction in Nonideal Crystals*, Springer-Verlag, Berlin, 1996. doi:https://doi.org/10.1007/978-3-642-74291-0.
- [19] G.K. Williamson, R.E. Smallman, III. Dislocation densities in some annealed and cold-worked metals from measurements on the X-ray Debye-Scherrer spectrum, *Philos. Mag.* 1 (1956) 34–46. doi:10.1080/14786435608238074.
- [20] A.R. Kil'mametov, R.Z. Valiev, R.K. Islamgaliev, G. V Nurislamova, Structural features of nanocrystalline nickel subjected to high-pressure torsion, *Phys. Met. Metallogr.* 101 (2006) 75–82. doi:10.1134/s0031918x06010108.
- [21] Z. Yang, U. Welzel, Microstructure-microhardness relation of nanostructured Ni produced by high-pressure torsion, *Mater. Lett.* 59 (2005) 3406–3409. doi:10.1016/j.matlet.2005.05.077.
- [22] L. Reinert, M. Zeiger, S. Suárez, V. Presser, F. Mücklich, Dispersion analysis of carbon nanotubes, carbon onions, and nanodiamonds for their application as reinforcement phase in nickel metal matrix composites, *RSC Adv.* 5 (2015) 95149–95159. doi:10.1039/C5RA14310A.
- [23] P. Scardi, M. Ortolani, M. Leoni, WPPM: Microstructural Analysis beyond the Rietveld Method, *Mater. Sci. Forum.* 651 (2010) 155–171. doi:10.4028/www.scientific.net/MSF.651.155.
- [24] M. Leoni, T. Confente, P. Scardi, PM2K: a flexible program implementing Whole Powder Pattern Modelling, *Zeitschrift Fur Krist. Suppl.* (2006) 249–254.

- [25] J. Martinez-Garcia, M. Leoni, P. Scardi, A general approach for determining the diffraction contrast factor of straight-line dislocations, *Acta Crystallogr. Sect. A Found. Crystallogr.* 65 (2009) 109–119. doi:10.1107/S010876730804186X.
- [26] P. Scardi, M. Leoni, M. D’Incau, Whole Powder Pattern Modelling of cubic metal powders deformed by high energy milling, *Zeitschrift Fur Krist.* 222 (2007) 129–135. doi:10.1524/zkri.2007.222.3-4.129.
- [27] A. Bachmaier, A. Hohenwarter, R. Pippan, New procedure to generate stable nanocrystallites by severe plastic deformation, *Scr. Mater.* 61 (2009) 1016–1019. doi:10.1016/j.scriptamat.2009.08.016.
- [28] J. Guo, M.J. Duarte, Y. Zhang, A. Bachmaier, C. Gammer, G. Dehm, R. Pippan, Z. Zhang, Oxygen-mediated deformation and grain refinement in Cu Fe nanocrystalline alloys, *Acta Mater.* 166 (2018) 281–293. doi:10.1016/j.actamat.2018.12.040.
- [29] K. Aristizabal, A. Katzensteiner, A. Bachmaier, F. Mücklich, S. Suárez, On the reinforcement homogenization in CNT/metal matrix composites during severe plastic deformation, *Mater. Charact.* 136 (2018) 375–381. doi:10.1016/j.matchar.2018.01.007.
- [30] D. Setman, E. Schafler, E. Korznikova, M.J. Zehetbauer, The presence and nature of vacancy type defects in nanometals detained by severe plastic deformation, *Mater. Sci. Eng. A.* 493 (2008) 116–122. doi:10.1016/j.msea.2007.06.093.
- [31] J. Kratochvil, S. Libovicky, Dipole drift mechanism of early stages of dislocation pattern formation in deformed metal single crystals, *Scr. Metall.* 20 (1986) 1625–1630.
- [32] A.A. Kusov, V.I. Vladimirov, The Theory of Dynamic Annihilation of Dislocations, *Phys. Status Solidi.* 138 (1986) 135–142. doi:10.1002/pssb.2221380114.
- [33] U. Essmann, H. Mughrabi, *Philosophical Magazine A*, *Philos. Mag. A.* 40 (1979) 731–756. doi:http://dx.doi.org/10.1080/01418617908234871.
- [34] M.J. Zehetbauer, J. Kohout, Principles and modeling of severe plastic deformation providing ultra fine grained materials, in: *Plast. Damage Fract. Macro, Micro Nano Scales*, *Plast. Int. Symp. Plast. Its Curr. Appl.* 9., NEAT Press, Fulton, 2002: pp. 543–545.
- [35] M.J. Zehetbauer, H.P. Stüwe, A. Vorhauer, E. Schafler, J. Kohout, The role of hydrostatic pressure in severe plastic deformation, *Adv. Eng. Mater.* 5 (2003) 330–337. doi:10.1002/adem.200310090.
- [36] M.J. Zehetbauer, Y. Estrin, Modeling of Strength and Strain Hardening of Bulk Nanostructured Materials, in: M.J. Zehetbauer, Y. Zhu (Eds.), *Bulk Nanostructured Mater.*, WILEY-VCH Verlag, 2009: pp. 109–136.

- [37] J. Gubicza, S. V. Dobatkin, E. Khosravi, A.A. Kuznetsov, J.L. Lábár, Microstructural stability of Cu processed by different routes of severe plastic deformation, *Mater. Sci. Eng. A.* 528 (2011) 1828–1832. doi:10.1016/j.msea.2010.11.026.
- [38] M. Zehetbauer, B. Jóni, G. Tichy, E. Schafner, T. Ungár, Correlation between the microstructure studied by X-ray line profile analysis and the strength of high-pressure-torsion processed Nb and Ta, *Acta Mater.* 61 (2012) 632–642. doi:10.1016/j.actamat.2012.10.008.
- [39] T. Ungár, G. Tichy, J. Gubicza, R.J. Hellmig, Correlation between subgrains and coherently scattering domains, *Powder Diffr.* 20 (2005) 366–375. doi:10.1154/1.2135313.
- [40] G.B. Rathmayr, R. Pippan, Influence of impurities and deformation temperature on the saturation microstructure and ductility of HPT-deformed nickel, *Acta Mater.* 59 (2011) 7228–7240. doi:10.1016/j.actamat.2011.08.023.
- [41] M.J. Starink, Dislocation versus grain boundary strengthening in SPD processed metals: Non-causal relation between grain size and strength of deformed polycrystals, *Mater. Sci. Eng. A.* 705 (2017) 42–45. doi:10.1016/j.msea.2017.08.069.
- [42] R.W. Armstrong, N. Balasubramanian, Unified Hall-Petch description of nano-grain nickel hardness, flow stress and strain rate sensitivity measurements, *AIP Adv.* 7 (2017) 1–6. doi:10.1063/1.4996294.
- [43] G.E. Dieter, Strengthening from fine particles, in: *Mech. Metall.*, McGraw-Hill, New York, USA, 1986: pp. 212–220.
- [44] J. Gubicza, Correlation between defect structure and mechanical properties of nanocrystalline materials, in: *Defect Struct. Prop. Nanomater.*, 2012: pp. 167–221.
- [45] J. Gubicza, Defect structure and mechanical properties of metal matrix–carbon nanotube composites, in: *Defect Struct. Prop. Nanomater.*, 2012: pp. 231–257.